JOURNAL OF GUIDANCE, CONTROL, AND DYNAMICS
Vol. 32, No. 5, September–October 2009

Optimal Deployment Control of Spinning Space Webs and Membranes

Mattias Gärdsback* and Gunnar Tibert†
Royal Institute of Technology, 100 44 Stockholm, Sweden

DOI: 10.2514/1.42203

Future solar sail and solar power satellite missions will consider using centrifugal forces for deployment and stabilization. Some of the main advantages with spin deployment are that the significant forces are in the plane of rotation, and a relatively simple control can be used and the tension in the membrane or web can be adjusted by the spin rate. Existing control strategies seem to either consume excessive energy or cause oscillations. In this study, control laws are derived from the solution to relevant optimal control problems and existing controls. The derived control laws are used in deployment simulations with both simple analytical three-degree-of-freedom models and a fully-three-dimensional finite element model. The results indicate that the derived control laws can be used to minimize the energy consumption and oscillations as for an optimal control, yet retain the simplicity of previous control laws.

Nomenclature

c	=	constant
$\boldsymbol{F}$	=	force vector
J	=	moment of inertia for the center hub
L	=	deployed length
$\mathcal{L}$	=	angular momentum
l	=	distance from the root of the arm to mass dm
M	=	torque applied to the hub
$\hat{M}$	=	torque constant in Melnikov–Koshelev laws
m_i	=	mass for part i
N	=	degree of Legendre polynomial
n	=	number of arms or nodes
$\boldsymbol{R}$	=	position vector
R	=	radius of the web or membrane
$\boldsymbol{r}$	=	radius vector
r	=	radius of the hub
S	=	side length of the web or membrane
s_i	=	sign of i
T	=	tensile force in the arm
$\boldsymbol{u}$	=	vector of control variables
$\boldsymbol{x}$	=	vector of state variables
α	=	$\phi + \varphi$
γ	=	power in the Melnikov–Koshelev power law
θ	=	rotation angle of the hub
ρ	=	density function
ϕ	=	coiling angle
φ	=	angle between the arm and the radial direction
ψ	=	threshold angle
ω	=	angular velocity (of the hub)

Subscripts

c	=	corner mass
f	=	final time
h	=	hub
t	=	tether
w	=	web or membrane
0	=	initial time

Superscript

i	=	coordinate system i

Introduction

LARGER and lighter structures are required for many space technologies (e.g., solar sails and solar power systems). Flexible structures have the potential to keep the weight and package volume small and be deployed to the required size in orbit [1]. One interesting method to deploy and stiffen flexible structures is to use the centrifugal force, which offers significant advantages compared with rigid alternatives [2]: low mass, small package volume, low deployment power consumption, possible gyroscopic repointing, acceptable surface accuracy, and presumably low cost.

In the early 1960s, Astro Research Corporation analyzed several large spin-stabilized space structures [3–8]. Two feasibility studies that provide important information are the Heliogyro solar sail [6], with flexible extendible rotor blades, and the large-aperture paraboloidal-reflector low-frequency telescope (LOFT) [4–8]. The first and only successful spin deployment of a large structure in orbit is the Russian 20-m-diam reflector Znamya-2 that was deployed in 1993 [9]. Six years later, the deployment of the 25-m-diam mirror in the follow-up experiment Znamya 2.5 failed because the membrane got caught in an antenna [10]. Spinning was considered in many of the early solar sail studies and recent spin concepts are developed for the Interstellar Probe Mission [11,12] and the UltraSail [13]. In 2004, the Japanese Institute of Space and Astronautical Science successfully demonstrated the deployment of a clover-type sail and a fan-type sail [14]. Several related concepts have been analyzed and tested both on ground and in space in Japan [15–20].

Space webs, in which spiderlike robots are used to build large structures on a web platform in orbit, were considered by Nakasuka et al. [21,22] for the Furoshiki satellite. The difficulty in deploying large structures in space was demonstrated in the Furoshiki experiment when the web entangled because of the rapid deployment and communication problems between the main satellite and the thrusters in the corners of the triangular web. With the aim to obtain a deployment that is easier to control, recent studies investigate the possibility to use the centrifugal force to deploy and stabilize webs in space [23–28].

Simple analytical models exist [8,9] in which the only degrees of freedom (DOF) are the center hub angular velocity, the length of the deployed web or arms, and the deviation angle of the web or arms

Received 14 November 2008; revision received 5 March 2009; accepted for publication 5 March 2009.

*Ph.D. Student, Department of Mechanics, Osquars Backe 18.
†Research Associate, Department of Mechanics, Osquars Backe 18; tibert@kth.se. Member AIAA (Corresponding Author).

relative to the radial axis. Multiparticle models with spring-mass networks have also been presented, with constants determined experimentally [14] and analytically [29]. Most membrane deployment models (e.g., [2,9,14]) focus on folding patterns for the deployment of split membranes with sections that can be folded on separate reels and be assembled after the deployment, even though Melnikov and Koshelev [9] also included a model for continuous membranes.

The present authors have recently presented a space web deployment concept including a prestressable web geometry and topology, a suitable folding pattern, and a two-step deployment scheme [23–26]. A recent study [28] shows that a one-step deployment from the same folding pattern is preferred if tether control is not used. The omission of the tethers decreases the risk of entanglement, but also decreases the redundancy for the system. An analytical model of the deployment of the first step of continuous quadratic space webs, folded into radial arms coiled around the center hub, and a finite element (FE) model implemented in the commercial software LS-DYNA, were also developed.

Existing control strategies for centrifugal deployment of membranes and webs have not been obtained by mathematical analysis. Contrary, extensive research has been performed on the dynamics and control of deployment and retrieval of tethered satellite systems (TSS), which can be used as inspiration for modeling the spin deployment of membranes. A recent literature review on the dynamics and control of nonelectrodynamic TSS was presented by Kumar [30]. Different optimal control methods have been used for a subsatellite connected to a shuttle in a Keplerian orbit. Bainum and Kumar [31] used linear optimal control theory based on an application of the linear quadratic regulator method. A Lyapunov-based approach was used by Fujii and Anazawa [32] for nonlinear optimal tension control. Barkow et al. [33] compared free deployment, deployment using Kissel's law, optimal control, and controlling chaos strategies. Williams [34] found optimal deployment and retrieval trajectories using direct transcription methods for different spin conditions and discusses various optimality criteria [35]. We observe that optimal control of TSS models includes less variables than centrifugal deployment; the orbital angular velocity is constant and no torque is applied.

The aim of this study is to find control strategies for the deployment of membranes and webs, coiled on spools or coiled around a center hub, that minimize the energy consumption and the presence of final oscillations. Because all the significant forces, both external and rotational inertia forces, are in the plane of rotation, it is enough to solve this problem in two dimensions, even though additional attitude control may be required to maintain the plane of rotation for a real case. The Legendre pseudospectral (PS) optimal control method [36,37] is used to find optimal controls for different optimality criteria. The Legendre PS method has previously been used to develop attitude trajectories for zero-propellant maneuvers for the International Space Station [38] and optimal deployment and retrieval of tethered satellites [34,35]. The three-DOF models [8,9,28] were chosen to describe the dynamics of the problem. New control laws, derived from the optimal control results and the control strategies in [8,9], are proposed. The new control laws are investigated with both the analytical model and a fully-three-dimensional FE model.

Existing Controls for Spin Deployment

Several studies [9,23,28,29,39] have shown that uncontrolled spin deployment, in which the uncoiling of the web from the hub is initiated by the initial spin and the system is left alone, leads to repeated coiling on and coiling off of the web to and from the hub. Some kind of control is therefore required.

Several control strategies for the deployment of membranes are described in literature. However, in most studies (e.g., [6,11,12,40]), the focus is not on the mathematical analysis of the deployment. These strategies were discussed in [28].

Hedgepeth [8] considered to use either the torque, the deployed length of the radial tethers, or the tensile force in the tethers as control parameters and concluded that a simple drag-brake type of control for the tethers is feasible with a simple two-step scheduling of the spin-up torque. This two-step scheduling consists of keeping the torque constant at approximately 200 Nm and the web tension constant until about 40% of the deployment is complete and then rapidly decreasing the torque to zero and at the same time decreasing the web tension. However, Hedgepeth [8] noted potentially detrimental oscillations after both the initiation of the deployment and the termination of the torque.

Melnikov and Koshelev [9] decided to use the torque applied to the center hub and the velocity of the spools, which the reflector parts are fed out from, as control parameters for the deployment of the Znamya-2 reflector. They investigated two control laws: 1) constant angular velocity, at which the coiling-off-and-on phenomenon would occur and 2) a torque with drooping characteristics, which ensures a stable deployment. The successful control law increases the torque applied to the hub as the angular velocity decreases:

$$M = \hat{M}\left(1 - \frac{\omega}{\omega_0}\right) \tag{1}$$

where ω_0 is equal to the initial angular velocity of the system and $\hat{M}$ is the maximum torque if $\omega \geq 0$. Henceforth, Eq. (1) is referred to as the Melnikov–Koshelev (MK) law. Melnikov and Koshelev [9] found that a higher value of the quotient $\hat{M}/\omega_0$ yields a more stable deployment. Using this strategy, a high initial angular velocity, a low final angular velocity, a short deployment time, and a stable and smooth deployment without entanglement and recoiling are obtained. Unlike tethers or split reflectors, as in [9], continuous space webs are cumbersome to feed out from spools. As a consequence, the deployment rate cannot be controlled by the spool velocity. However, by folding the web into arms and then coiling them around the center hub, the deployment rate is determined and controlled by the hub spin [28].

To apply the torque, Melnikov and Koshelev [9] proposed to use an electric motor that spins up a counter-rotating system. Because of conservation of angular momentum, the hub–web system spins the other way around. The counter-rotating system (e.g., a flywheel) also stores the kinetic energy, spin-stabilizes the whole system, and can be used for reorientation of the spinning space web.

The main advantage with the MK law is that it is not directly linked to the analytical model, and therefore it is less dependent on the model accuracy. Sufficient agreement between the analytical model and the real behavior is required to determine suitable values of the parameters $\hat{M}$ and ω_0, but this type of control includes feedback correction on its own because it adjusts the torque based on the measured value of ω. The disadvantage is that torque is continuously applied until $\omega = \omega_0$ again, which is energy consuming and requires increased material strength because both the kinetic energy and the centrifugal force are proportional to ω^2. Alternatively, the torque must be turned off before the arms are in the radial direction, which induces oscillations that are approximately proportional to the angle relative to that direction [28]. A control law that enables a low final angular velocity, yet deploys the web without oscillations, is required.

Dynamic Model

A relatively simple analytical model is required to describe the dynamics of the problem to compute the optimal control and the optimal trajectory in reasonable time. Two-dimensional models with only three DOF have been used to describe the dynamic deployment behavior for star folded webs [28] and membranes [9]. The results for such models show good agreement with more advanced FE models [28] as long as the arms are straight and the deployment is slow enough to not include elasticity, which is true for most relevant controlled deployments. A similar model was also used by Hedgepeth [8] to describe the LOFT deployment (Fig. 1), and hub-wrapped membranes can be described with similar models [23]. The model does not differentiate between membranes and webs or between separate arms and strings of a continuous membrane or web,

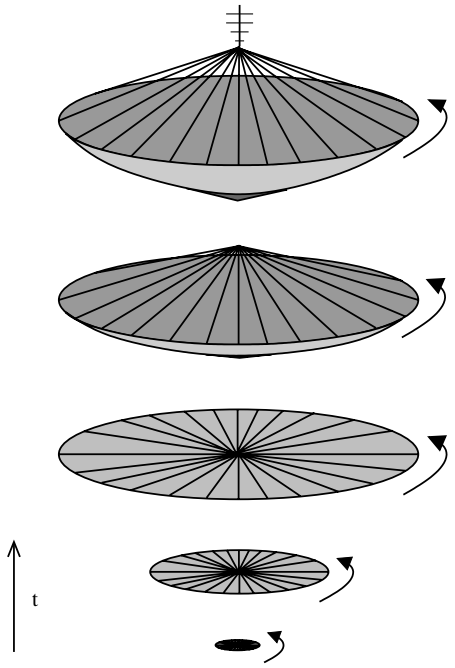

Fig. 1 LOFT deployment.

and so in the following they are denoted as membranes and arms, respectively. The DOF are the angular velocity of the center hub, the deviation angle of an arm relative to the radial direction, and the current length of the arm. The angular velocity of the center hub, not the orientation, is used as a DOF, because its exact position is not of interest. For membranes coiled around the hub, the deviation angle is instead the angle that the membrane is coiled around the hub and the current length of the arm is directly related to the angle.

The following assumptions were made for the analytical centrifugal hub–membrane model [28]:

1) Effects of gravity or orbit or hub direction in the orbit were not considered.

2) Out-of-plane motions were not included.

3) The arms were supposed to be straight and deployed symmetrically relative to the central axis.

4) The elasticity in the membrane was neglected.

5) Energy dissipation caused by deformation, friction, and environmental effects was neglected.

The effects of a gravity gradient are negligible during the time of deployment [9]. Out-of-plane motions could be a problem initially, when the rotational inertia forces are small, but the folding and initial velocity should be chosen so that these motions are minimized. Assumptions 3 and 4 hold for relevant controls [28]. Energy dissipation could occur and is difficult to quantify, but it will only contribute to damp out oscillations.

Similar models have also been used for optimal control of tether deployment and retrieval of a subsatellite from a shuttle in Keplerian orbit [32–35]. Even though tether deployment and centrifugal deployment of membranes are different in reality, the mathematical formulations are similar: the point at which an arm is attached to the center hub corresponds to the shuttle and the end mass corresponds to the tethered subsatellite. The differences between the models are that the tether model assumes constant angular velocity for the shuttle in orbit and includes the gravitational potential, whereas the change of angular velocity is essential for the centrifugal hub–membrane model but the gravitational forces can be neglected, compared with the centrifugal forces.

Equations for Straight Arms

Three equations are required to solve for the three unknown DOF. Here, the change of angular momentum for the hub and two equations of motion for the arms in the plane of rotation are available.

The change in angular momentum, due to the applied external torque and the torque exerted by the pulling arms, for the central hub in Fig. 2 is

$$\dot{\mathcal{L}} = \boldsymbol{M} + n(\boldsymbol{r} \times \boldsymbol{F}) \tag{2}$$

Projected along the axis of rotation it becomes

$$J\dot{\omega} = M + nTr\sin\varphi \tag{3}$$

Note that J is not constant if the web is deployed from the hub and out. Summing the contributions from all small masses dm along an arm, the equations of motion become

$$\int_0^L \ddot{\boldsymbol{R}}\rho(l)\mathrm{d}l = \boldsymbol{F} \tag{4}$$

where $\ddot{\boldsymbol{R}}$ is obtained from Fig. 2 as

$$\boldsymbol{R} = \boldsymbol{r} + \boldsymbol{l} \tag{5}$$

and the derivatives of $\boldsymbol{R}$ become

$$\dot{\boldsymbol{R}} = \boldsymbol{\omega} \times \boldsymbol{r} + \boldsymbol{l}' + (\boldsymbol{\omega} + \dot{\varphi}\boldsymbol{e}_3^{(2)}) \times \boldsymbol{l} \tag{6}$$

$$\ddot{\boldsymbol{R}} = \dot{\boldsymbol{\omega}} \times \boldsymbol{r} + \boldsymbol{\omega} \times (\boldsymbol{\omega} \times \boldsymbol{r}) + \boldsymbol{l}'' + 2(\boldsymbol{\omega} + \dot{\varphi}\boldsymbol{e}_3^{(2)}) \times \boldsymbol{l}' + (\dot{\boldsymbol{\omega}} + \ddot{\varphi}\boldsymbol{e}_3^{(2)}) \times \boldsymbol{l} + (\boldsymbol{\omega} + \dot{\varphi}\boldsymbol{e}_3^{(2)}) \times ((\boldsymbol{\omega} + \dot{\varphi}\boldsymbol{e}_3^{(2)}) \times \boldsymbol{l}) \tag{7}$$

where prime denotes derivation in the local coordinate system (2). For a general case, in which the model assumptions are valid, the equations of motion become

$$a[r(\omega^2\cos\varphi - \dot{\omega}\sin\varphi) - \ddot{L}] + b(\omega + \dot{\varphi})^2 = nT \tag{8}$$

$$a[r(\dot{\omega}\cos\varphi + \omega^2\sin\varphi) + 2\dot{L}(\omega + \dot{\varphi})] + b(\dot{\omega} + \ddot{\varphi}) = 0 \tag{9}$$

where the functions a and b depend on $\rho(l)$ for the chosen folding pattern and membrane geometry. For arm deployment of a quadratic membrane with corner masses [23,28], a and b are

$$a = a(L) = m_c + \frac{m_w L^2}{L_{\max}^2} \tag{10}$$

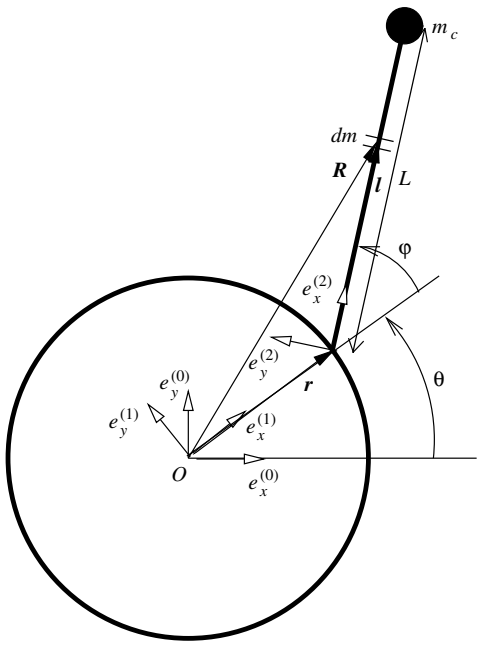

Fig. 2 The analytical model for a point mass or mass distributed over the arm length.

$$b = b(L) = L\left(m_c + \frac{m_w L^2}{3L_{\max}^2}\right) \tag{11}$$

where $L_{\max} = S/2 - \pi r/n$. Because n is included on the right-hand side of Eq. (8), m_c is the total mass of all corners, not the mass in each corner. For a split circular membrane [9] or its continuous equivalent, a hub-wrapped circular membrane [23], a and b become

$$a = a(L) = \frac{m_w L}{L_{\max}^2}(2L_{\max} - L) \tag{12}$$

$$b = b(L) = \frac{m_w L^2}{L_{\max}^2}\left(L_{\max} - \frac{L}{3}\right) \tag{13}$$

where $L_{\max} = R - r$. Note that this does not give a perfect circle, but close enough if $R \gg r$. For LOFT [8],

$$a = a(L) = m_c + m_t + \frac{2m_w L}{L_{\max}^2}\left(L_{\max} - \frac{L}{2}\right) \tag{14}$$

$$b = b(L) = L\left[m_c + \frac{m_t}{2} + \frac{m_w L}{L_{\max}^2}\left(L_{\max} - \frac{L}{3}\right)\right] \tag{15}$$

where $L_{\max} = R - r$. Evidently, Eqs. (8) and (9), with the appropriate expressions for a and b, can also be used for a point mass, where $m_w = m_t = 0$, or if there are no corner masses (i.e., $m_c = 0$). Similar expressions for the functions a and b can be obtained for different folding patterns [9,23].

Equations for Arms Coiled Around the Hub

For a web or membrane that is coiled around the hub (Fig. 3), only two DOF, ω and the coiling angle ϕ, are required because L is given by

$$L = L_{\max} - r|\phi| \tag{16}$$

Because T is unknown, three equations are still required. The equations are [28]

$$J\dot{\omega} = M + s_\phi nTr \tag{17}$$

$$-s_\phi ar\dot{\omega} + b(\omega + \dot{\phi})^2 = nT \tag{18}$$

$$s_\phi ar(\omega^2 - \dot{\phi}^2) + b(\dot{\omega} + \ddot{\phi}) = 0 \tag{19}$$

where L in a and b are replaced with Eq. (16).

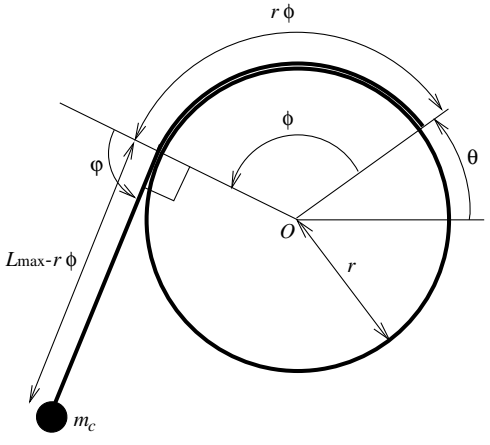

Fig. 3 The analytical model for an arm coiled around the hub.

Dynamic Constraints for Arms Coiled onto Spools

If the membrane is deployed from spools on the tip of the arms, as in [9], or in separate parts from spools at the center hub, as in [8], then both N and M are used to control the deployment. The vector of state variables is

$$\boldsymbol{x} = \left(x_1, x_2, x_3, x_4, x_5\right)^T = \left(\omega, \varphi, \dot{\varphi}, L, \dot{L}\right)^T \tag{20}$$

and the vector of control variables is

$$\boldsymbol{u} = \left(u_1, u_2\right)^T = \left(M, nT\right)^T \tag{21}$$

and the governing equations can be written as a system of nonlinear ordinary differential equations:

$$\dot{\boldsymbol{x}} = \begin{pmatrix} \dot{\omega} \\ x_3 \\ -\dot{\omega} - \dfrac{a}{b}[r(\dot{\omega}\cos x_2 + x_1^2 \sin x_2) + 2x_5(x_1 + x_3)] \\ x_5 \\ r(x_1^2 \cos x_2 - \dot{\omega}\sin x_2) + \dfrac{b}{a}(x_1 + x_3)^2 - \dfrac{u_2}{a} \end{pmatrix} \tag{22}$$

where

$$\dot{\omega} = \frac{u_1 + ru_2 \sin x_2}{J} \tag{23}$$

Dynamic Constraints for Arms Coiled Around the Hub

If the arms are coiled around the center hub, only two DOF, corresponding to three state variables, are required. The vector of state variables is

$$\boldsymbol{x} = \left(x_1, x_2, x_3\right)^T = \left(\omega, \alpha, \dot{\alpha}\right)^T \tag{24}$$

where we have introduced the variable

$$\alpha = \phi + \varphi \tag{25}$$

because coiled arms become straight when they are completely coiled off. It is not possible to control the coiling-off rate directly. Therefore, the vector of control variables is simply a scalar:

$$\boldsymbol{u} = u_1 = M \tag{26}$$

As shown in the previous sections, different equations are used to describe the deployment when the arms are partially coiled around the hub and when the arms are straight. If $|\alpha| < \pi/2$ (i.e., the arms are straight), the system of ordinary differential equations to solve are derived from Eqs. (3), (8), and (9):

$$\dot{\boldsymbol{x}} = \begin{pmatrix} \dot{\omega} \\ x_3 \\ -\dot{\omega} - \dfrac{a}{b} r(\dot{\omega}\cos x_2 + x_1^2 \sin x_2) \end{pmatrix} \tag{27}$$

where

$$\dot{\omega} = \frac{u_1 + r\sin x_2(arx_1^2 \cos x_2 + b(x_1 + x_3)^2)}{J + ar^2 \sin^2 x_2} \tag{28}$$

Instead, if $\alpha < -\pi/2$ (i.e., the arms are coiled clockwise around the hub), then

$$\dot{\boldsymbol{x}} = \begin{pmatrix} \dot{\omega} \\ x_3 \\ -\dot{\omega} + \dfrac{a}{b} r(x_1^2 - x_3^2) \end{pmatrix} \tag{29}$$

where

$$\dot{\omega} = \frac{u_1 - br(x_1 + x_3)^2}{J + ar^2} \tag{30}$$

and L in a and b is given by

$$L = L_{\max} + r\left(x_2 + \frac{\pi}{2}\right) \tag{31}$$

Finally, if $\alpha > \pi/2$ (i.e., the arms are coiled counterclockwise), the differential equations are obtained analogously as for $\alpha < \pi/2$ from Eqs. (17–19).

Optimization

The goal of this study is to find control laws that bring the dynamic systems in the previous section from the folded configuration to a configuration close to a final steady state without exceeding certain upper and lower limits for the control and state variables.

Problem Formulation

A general optimal control problem is to minimize the Bolza cost function

$$\min_{\boldsymbol{u}\in U} \int_{t_0}^{t_f} F(\boldsymbol{x}(t), \boldsymbol{u}(t), t)\mathrm{d}t + G(\boldsymbol{x}(t_0), t_0, \boldsymbol{x}(t_f), t_f) \tag{32}$$

subject to some dynamic constraints

$$\frac{d\boldsymbol{x}}{dt} = \boldsymbol{f}(\boldsymbol{x}(t), \boldsymbol{u}(t), t) \tag{33}$$

boundary conditions

$$\boldsymbol{g}\,(\boldsymbol{x}(t_0), t_0, \boldsymbol{x}(t_f), t_f) = \boldsymbol{0} \tag{34}$$

and inequality path constraints

$$\boldsymbol{h}\,(\boldsymbol{x}(t), \boldsymbol{u}(t), t) \leq \boldsymbol{0} \tag{35}$$

where $\boldsymbol{x}(t)$ is defined in Eq. (20) or Eq. (24) and $\boldsymbol{u}(t)$ is defined in Eq. (21) or Eq. (26).

Optimal Control Methods

Optimal control problems can be solved by either indirect or direct methods. For the present problem, it is possible to obtain the optimality conditions required for indirect methods, but the result is a multipoint boundary value problem that is very complicated to solve. Direct methods directly discretize the continuous optimal control problem and transcribe it into a parameter optimization problem that can be solved using standard nonlinear programming (NLP) tools [41]. Direct transcription of optimal control problems requires approximations of the integration in the cost function, the differential equations of the state-control system, and the state-control constraint equations, and, ideally, the same collocation points should be used for all.

One possibility is to use PS methods, which converge with spectral accuracy for smooth problems [42] and are efficient for all the three approximations, as proved in [43]. All PS methods use an orthogonal polynomial of degree N evaluated at $N + 1$ points. The points are usually the $N - 1$ roots of the polynomial and the boundaries of the domain $[-1, 1]$. Exact integration for a polynomial of degree N is obtained for this set of points.

The Legendre PS (LPS) method is the most widely used PS method because of its proven convergence properties and because it is possible to accept or reject solutions based on the optimality conditions [43]. In LPS, Lagrange interpolation polynomials, based on the Legendre polynomial of degree N, are used to derive trial functions that connect the continuous and discrete state and control variables. The Legendre–Gauss–Lobatto points are used as collocation points. The Gauss–Lobatto quadrature rule is used for the integration of the objective function. The LPS method is available in the MATLAB-based commercial code DIDO [44]. Here, the problem was instead solved directly in the Comsol script [45] because the implementation of the algorithms is rather straightforward. The NLP problem was solved using the SNOPT-based [46] Comsol Optimization Lab [47].

Choice of Objective Function, Boundary Conditions, and Path Constraints

An optimal control is only optimal with respect to its optimization criteria. Different optimality criteria for the deployment and retrieval of tethered satellites, using elastic and inelastic tether models, were discussed by Williams [35], who found that it is important to minimize the length acceleration, the tension rate, and the tension acceleration. These conclusions are valuable, but for spin deployment of membranes, the torque application is very important and elasticity of the web is less important.

An optimal spin deployment should 1) cause a minimum of oscillations in the end and 2) require a minimum of control efforts, which could be to minimize the maximum power or torque, or minimize the total energy consumption or total change of angular momentum, or a combination. A third requirement could be that it should be completed within a specified time. Complete deployment is obtained when 1) the membrane has reached its full size, $L = L_{\max}$, 2) the system is spinning with the desired angular velocity, $\omega = \omega_f$, and 3) the system is in steady state, $\dot{L} = \alpha = \dot{\alpha} = 0$.

Note that if a control law can be found so that the path constraint $M(t) \geq 0$ (for all t) holds, and the final state $L = L_{\max}$, $\omega = \omega_f$, and $\alpha = 0$ at $t = t_f$ is obtained and is in steady state, then the control law for M minimizes both the integrals

$$\int_0^{t_f} M\mathrm{d}t \tag{36}$$

and

$$\int_0^{t_f} M\omega\mathrm{d}t \tag{37}$$

(i.e., the increase of angular momentum and kinetic energy), because a surplus of angular momentum and energy would give oscillations if damping is not present, and a deficit of them would not give full deployment at the desired final angular velocity. This implies that any solution that fulfills this is optimal in this sense, but it also implies that the solution is not unique, as will be shown in the results.

The parameters $\dot{\alpha}$ and ω are also closely interconnected. This suggests that relevant optimal problems are to minimize $\ddot{\alpha}$ and $\dot{\omega}$ or the integral of the applied torque or power, together with constraints on the final state. Unfortunately, neither of these attempts converged for the present problem and a compromise had to be selected.

Quadratic criteria are preferred because the existence of derivatives and the second derivatives of the objective function improves the convergence properties, especially if the control variables are included. However, for minimum-fuel problems it has been shown [48,49] that quadratic objective functions are less efficient than to actually minimize the energy consumption, which can often be achieved with bang–bang control. On the other hand, quadratic criteria render smooth curves for the control variables, which is an advantage compared with bang–bang control for centrifugal deployment for at least two reasons:

1) A time lag from the commanded to the real torque application has less significance.

2) Oscillations, which are difficult to damp out, may be induced with bang–bang control.

Also, squared integrands can be interpreted as combinations between the mean and the maximum values, which is useful here.

Performance indices that were considered as part of the objective function are listed in Table 1. Different optimization criteria are suitable for membranes folded around the hub and for those folded onto spools, because different state and control variables are used. Also, different criteria are suitable for the deployment phase, where $L \to L_{\max}$, and the stabilization phase, where $\alpha \to 0$, but because it is difficult to a priori determine the phase shift, the same criterion is preferably used for both phases. In reality, $t_f = \infty$, but for computational reasons it is sufficient to truncate the integrals and choose a suitable t_f. To obtain convergence, it seems better to not include the final state in Eq. (34) and to instead make it part of the objective function. Possible explanations may be the oscillatory

Table 1 Optimization criteria

Weight	Objective function	Description
w_1	$\int_{t_0}^{t_f}(\omega-\omega_f)^2\mathrm{d}t$	Squared deviation from the desired final angular velocity
w_2	$\int_{t_0}^{t_f}\alpha^2\mathrm{d}t$	Squared angular deviation from the radial direction
w_3	$\int_{t_0}^{t_f}\dot{\alpha}^2\mathrm{d}t$	Squared arm oscillations
w_4	$\int_{t_0}^{t_f}(L-L_{\max})^2\mathrm{d}t$	Squared deviation from fully deployed length
w_5	$\int_{t_0}^{t_f}\dot{L}^2\mathrm{d}t$	Squared spool oscillations
w_6	$\int_{t_0}^{t_f}M^2\mathrm{d}t$	Squared torque
w_7	$\int_{t_0}^{t_f}N^2\mathrm{d}t$	Squared arm tension
w_8	$\int_{t_0}^{t_f}(M\omega)^2\mathrm{d}t$	Squared power
w_9	$\int_{t_0}^{t_f}M\mathrm{d}t$	Total applied angular momentum
w_{10}	$\int_{t_0}^{t_f}M\omega\mathrm{d}t$	Total applied energy
w_{11}	$(\int_{t_0}^{t_f}M\mathrm{d}t-(\mathcal{L}_f-\mathcal{L}_0))^2$	Deviation from required angular momentum
w_{12}	$(\int_{t_0}^{t_f}M\omega\mathrm{d}t-(\mathcal{K}_f-\mathcal{K}_0))^2$	Deviation from required energy
w_{13}	$\ddot{\alpha}(t_f)$	Final oscillation of the arm
w_{14}	$\dot{\omega}(t_f)$	Final oscillation of the hub

behavior, or the rapidly changing dynamics, of the deployment. Objective function 6 in Table 1 does not exactly minimize the angular momentum, but was chosen because its superior convergence properties compared with functions 8–12. Function 4 is required to obtain complete deployment. Function 1 is required to get the desired ω_f. It seems natural to use minimization of the difference compared with the desired final values only at the final time step, but all such attempts failed to converge.

For membranes coiled around the center hub, the initial conditions are $\omega(t_0)=\omega_0$ and

$$\alpha(t_0)=\phi(t_0)+\varphi(t_0)=-\pi/2-(L_{\max}-\epsilon)/r_0$$

If they are instead coiled on spools, $\omega(t_0)=\omega_0$, $\alpha(t_0)=0$, and $L=\epsilon$. The parameter ϵ is small, but required to start the deployment. In both cases, $\dot{\alpha}(t_0)$ is arbitrary.

Path constraints must be imposed on the state variables: L is restricted to $0\le L\le L_{\max}$ because of the arm length, and $\omega>0$ is required because changed hub rotation often cause an unstable deployment [28]. For deployment from spools, $|\alpha|<\pi/2$ is required to avoid coiling onto the hub and $|\alpha|<\pi/6$ decreases the risk of entanglement [9]. Some path constraints may also be imposed on the control variables. The torque should have the same sign as ω, because energy is wasted if the torque is applied in the direction opposite to the hub rotation. In reality, there is also a maximum torque of the electric motor, but here it was considered more interesting to observe how the choice of objective function affected the torque. T is a tensile force (i.e., $T>0$) and its upper limit can possibly be chosen as the static force (i.e., the force when the web is completely deployed). However, it is better to omit the upper constraint and instead reduce the initial angular velocity if T becomes too high. All these limitations can be included in Eq. (35). However, it may occasionally be necessary to allow slightly larger or smaller values to obtain convergence.

Initial Guess and Scaling

A sequential quadratic programming (SQP) algorithm was used to solve the NLP problem. Because SQP algorithms search for locally optimal solutions, it is essential to provide an initial guess for the state and control variables at the collocation points that is sufficiently close to the optimal solution. Furthermore, the initial guess must be sufficiently smooth, which may be a problem for centrifugal force deployment because of its inherently oscillatory behavior. The results from a simulation using the MK law fulfill both these demands.

Scaling could improve the convergence of NLP solvers. Attempts were therefore performed to scale the length and time scales so that as many state and control variables as possible had maximum values near 1. However, no improvement of the computational time was achieved. Instead, the main computational problem here was to determine $\ddot{\alpha}$ from the dynamic equations, especially if ω is much greater. This cannot be improved by scaling. Furthermore, all constraints and variables were scaled automatically by Comsol's SNOPT-based NLP solver [47] using an iterative procedure that attempts to make the matrix coefficients as close as possible to 1.0.

Finite Element Model

The analytical model cannot accurately describe one-step deployment of space webs. Therefore, a three-dimensional finite element model, including a center hub, a web, and four corner masses, was implemented and solved using explicit time integration in LS-DYNA [50]. The model was described in detail in [28]. The main differences compared with the analytical model are that other deployment sequences than arm deployment can be studied with the FE model, the arms are not necessarily straight during the deployment, the cables can store elastic energy, and perturbations can be studied. Gravity gradients, energy dissipation, and orbit effects can be included, but have been considered to be small for membranes in comparison with the rotational forces [9] and should be even smaller for a web.

The model of the initial folded configuration is very important as it provides the initial geometry and the initial velocities that determine the deployment sequence, deployment rate, and control requirements. The governing equations of the folding scheme were given in [23]. The size of the hub in the FE model is dependent on the mesh width of the web for reasons of folding and hub–web interaction [23]. In reality, the mesh width of the web would be, at most, 30 mm, whereas a significantly larger mesh width, 2.5 m, was used in the FE model for computational efficiency. The contact between the cables and the rigid center hub was modeled using the kinematic constraint method, which implies that cables in contact with the hub follow the hub. Contact between the cable elements was disregarded, because higher priority was given to coiling the space web as close to the center hub as possible.

Feedback control requires special treatment in FE codes because of the dependence on the current state. In the object version of LS-DYNA, the user can implement a function in the source code that applies a force to selected shell or beam elements. To apply the control torque, four planar shells with negligible mass were symmetrically positioned in the center hub and force couples corresponding to the desired torque were applied to the peripheral nodes of the shells.

Results for Deployment of Webs and Membranes Coiled Around the Hub

In this section, the arm deployment for the quadratic space web introduced in [23,28], and described by the dynamic constraints in Eqs. (22) and (27) and the constants in Eqs. (10) and (11), serves as an example of a web or membrane folded in the arms and coiled around

the center hub and therefore controlled only by the torque applied to the hub.

The following data were used: the side length $S = 100$ m, the mass of the center hub $m_h = 100$ kg, the radius of the center hub $r = 6.3$ m, the mass of the web $m_w = 122$ kg, and the total mass of all four corners $m_c = 4$ kg. The web mass was obtained by assuming that the cables were made of the Zylon fibers in [51] and that the mesh width was 30 mm. For the FE model, the elastic modulus of the Zylon cables $E_{ca} = 180$ GPa, the density of the cables $\rho_{ca} = 1540$ kg/m^3, the cross-sectional area of the cables $A_{ca} = 2.5/0.030 \times 0.123$ mm^2, and the mesh width 2.5 m were also included. The cross-sectional area was adjusted so that the total mass of the web in the FE model was equal to that of a real web with 30 mm mesh width. The initial and final spin rates were chosen as $\omega_0 = \pi/10$ and $\omega_f = \pi/50$, respectively.

The dynamic equations in the analytical models were solved in MATLAB [52] using the ordinary differential equation solver ode45, with an estimated relative error less than 0.001 in each integration step. The FE model consisted of approximately 5000 active DOF and was solved in LS-DYNA using explicit integration and time steps of size 1.14×10^{-4} s. The time step of the FE had to be small, at least initially, because of the contact algorithm. The SQP problems, which were derived from the optimal control problems, were solved in Comsol Optimization Lab [47] with function tolerances and variable tolerances equal to 1×10^{-8}.

Deployment Using the MK Law

The MK law was used in [28] to control the deployment of the quadratic space web, initially coiled around the center hub. The problem with this control law is that excessive torque is required to not induce oscillations (Fig. 4). A control law that eliminates or decreases any oscillations is a requirement to obtain a tensioned web.

Optimal Control of the Deployment

The choice of objective function was extremely important both for the convergence and results of tested optimal control problems. For cases 1 and 2 in Fig. 5, the objective was to minimize the integral of the squared torque and the squared difference $L - L_{max}$, with $w_6 = w_3 = 1$ and all other weights in Table 1 equal to zero. The constraints on the state and control variables also had a significant impact on the results. The difference between cases 1 and 2 is that ω was allowed to fall to half the value in case 1 ($\omega_{min} = \pi/20$) compared with case 2 ($\omega_{min} = \pi/10$). Case 3 used the same constraints as case 2, but the objective was to minimize a combination between the squared torque ($w_6 = 1$) and the squared differences $L - L_{max}$ ($w_3 = 1$) and $\omega - \omega_f$ ($w_1 = 10^3$). The Legendre polynomial of order 63 was used for the discretization in Fig. 5, and of order 31 was used for verification of the convergence.

All three optimal control curves suggest that no torque should be applied initially, then the torque should be increased rapidly to prevent the center hub from changing its direction of rotation. After reaching its maximum value, torque should be applied to keep the center hub rotating faster than the lowest acceptable level, $\omega = \omega_{min}$. Finally, the torque should be turned off slowly until the angular momentum is sufficiently high to keep the system rotating at the desired angular velocity.

Derivation of New Control Laws from the Optimal Control Results

One main advantage with the MK law is that it is directly applicable, with appropriate parameters, to centrifugal deployment using folding patterns and deployment sequences that are difficult to model accurately (e.g., the one-step deployment of space webs used in [28]). The reason is that the MK law is not directly derived for a specific model, but is based on the simple idea that more torque is required if ω is low, thus making the torque linearly decreasing with increasing ω. The optimal control results suggest a nonlinear control torque that is smaller than the MK law when $\omega \gg 0$ and increases more rapidly when $\omega \to 0$. Another advantage is that additional torque may be required to force a system to follow an optimal trajectory if an inaccurate model was used to compute the optimal trajectory. Additional torque may also be required for the MK law if $\omega < \omega_{min}$, but the risk for this can be considerably decreased by careful parameter selection.

To resemble the optimal control torque more, while keeping the simplicity, a power of the ω-dependent factor in the MK law was introduced:

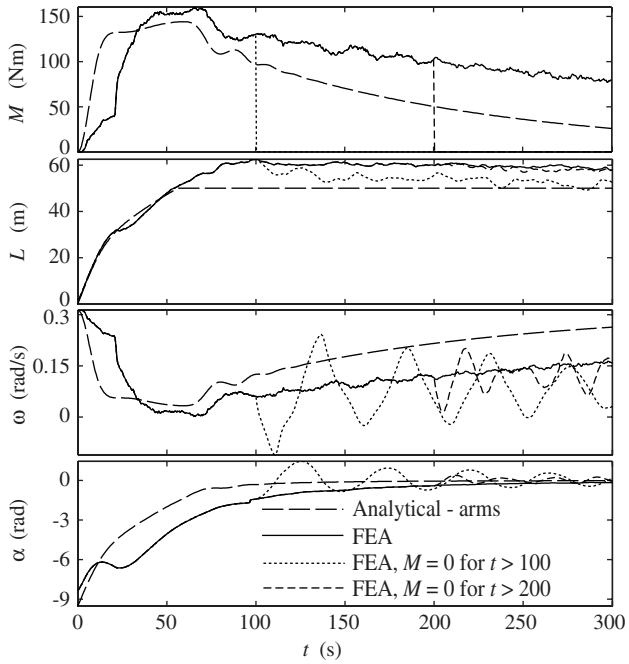

Fig. 4 Deployments of the quadratic space web in which torque is rapidly turned off (FEA denotes finite element analysis).

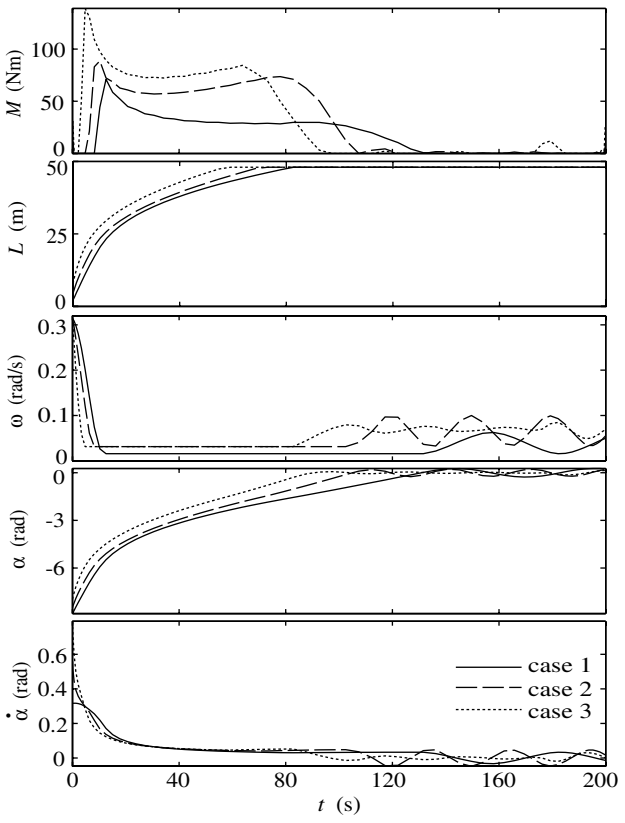

Fig. 5 Optimal control of space web deployment.

$$M = \hat{M}\left(1 - \frac{\omega}{\omega_0}\right)^{\gamma} \tag{38}$$

The parameter γ should be sufficiently large to give a small ω_f, yet sufficiently small to restrain the decrease of ω in the initial deployment phase. Equation (38) is henceforth denoted as the MK power law. Small, rapidly changing values of ω increase the risk of getting a noncontrollable deployment, especially if there is a significant lag from the measurement of ω, via the computer unit, to the torque application by the electric motor.

The main disadvantage with the MK power law is that it does not include the final angular velocity. A different or supplementary control law is therefore required to reach the desired final spin rate. One option is to replace ω_0 with ω_f and ensure that M is nonnegative:

$$M = \max\left[0, \hat{M}\left(1 - \frac{\omega}{\omega_f}\right)\right] \tag{39}$$

Equation (39) is denoted as the modified MK law. For this law, $M = 0$ if $\omega \geq \omega_f$ (i.e., in the initial and final phases of the deployment).

Simulations Using the New Control Laws

Simulation results using the MK power law with $\hat{M} = 50$ or 200 Nm, $\omega_0 = \pi/10$ rad/s, and $\gamma = 1$ or 10 are shown in Fig. 6. The larger value of γ required lower torque and gave a lower final angular velocity, given that the torque was turned off as soon as α was sufficiently small to not induce large oscillations, and thus the total angular momentum and energy consumption decreased substantially. If only L is observed, the deployment time increased slightly for a larger γ, but taking into account that a web is in tension only when α is close to zero, then the deployment time decreased. Another advantage of an increased γ is that it is much less sensitive to the choice of $\hat{M}$. When $\hat{M}$ was decreased by a factor 4, so that ω decreased to almost 0, then the angular velocity decreased below 0 for $\gamma = 1$ and oscillations were induced, whereas no oscillations occurred for $\gamma = 10$. Also, the maximum torque required for different $\hat{M}$ changed less for $\gamma = 10$ than for $\gamma = 1$.

The modified MK law is interesting because it ensures that $\omega = \omega_f$ at the end of the deployment. Results from simulations using the modified MK law with four different $\hat{M}$ are shown in Fig. 7. For the smallest $\hat{M}$, ω decreased to 0, which is a potential cause of instability. For the largest $\hat{M}$, excessive angular momentum was supplied to the system, which inevitably gave rise to oscillations, because no energy dissipates in the model and very little in reality. The amplitude of the oscillations was proportional to the surplus of angular momentum in the system compared with the angular momentum for a uniform rotation at $\omega = \omega_f$. The consequence is that $\hat{M}$ must also be chosen carefully for the modified MK law. Finally, note the close resemblance between the control torque for the MK power law with $\hat{M} = 50$ and $\gamma = 10$, the modified MK law with $\hat{M} = 50$, and the optimal control (Fig. 8).

Optimal Control of Only the Stabilization Phase

It is not certain that ω_f is reached for the MK law, for the MK power law, and for many optimal controls in which the focus is on the deployment phase (i.e., the coiling off of the arms from the hub). Even though no such results were obtained, it should be noted that it can be efficient to use a separate optimal control for the stabilization phase (i.e., when $|\alpha| \leq \pi/2$).

Finite Element Simulations

For one-step deployment of space webs, LS-DYNA was used to test 1) the MK power law (with $\gamma = 10$), 2) the modified MK law, and 3) the MK law. $\hat{M} = 200$ Nm was used for all three laws. The MK power law and the modified MK law showed similar results (Fig. 9). Higher torque, both maximum and mean, was required for the original MK law than for the two new laws. The main consequence of this is that ω_f became higher than desired for the MK law and was

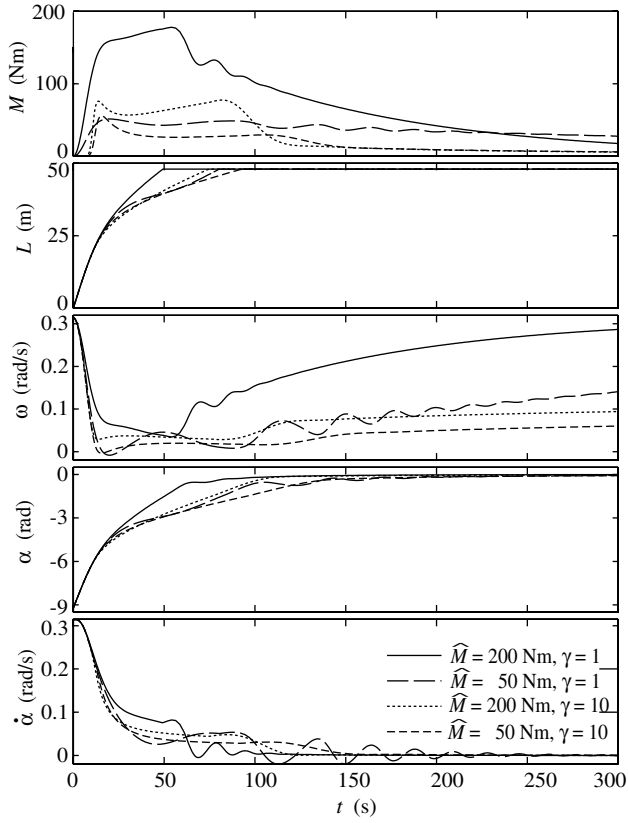

Fig. 6 Space web deployment using the MK power law with different $\hat{M}$ and γ.

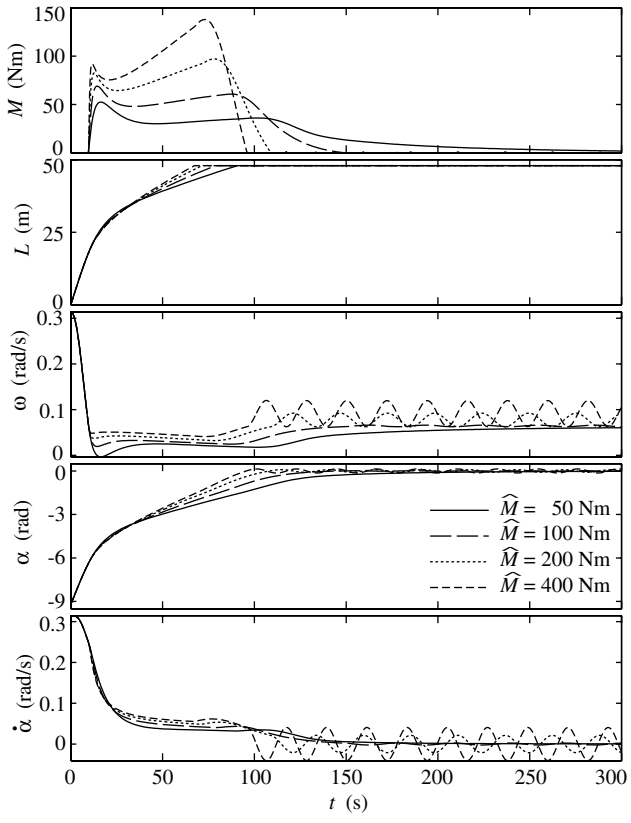

Fig. 7 Space web deployment using the modified MK law with different $\hat{M}$.

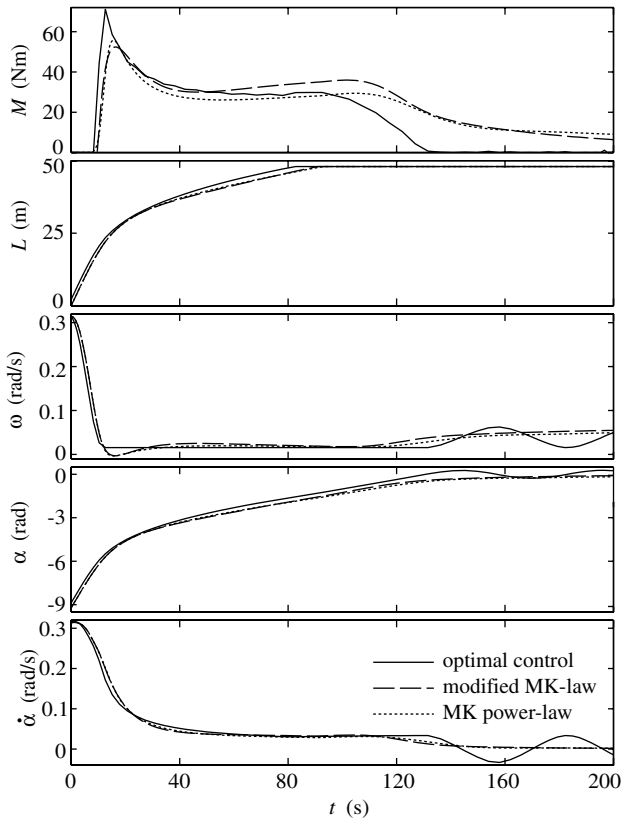

Fig. 8 Comparison of control laws for space web deployment.

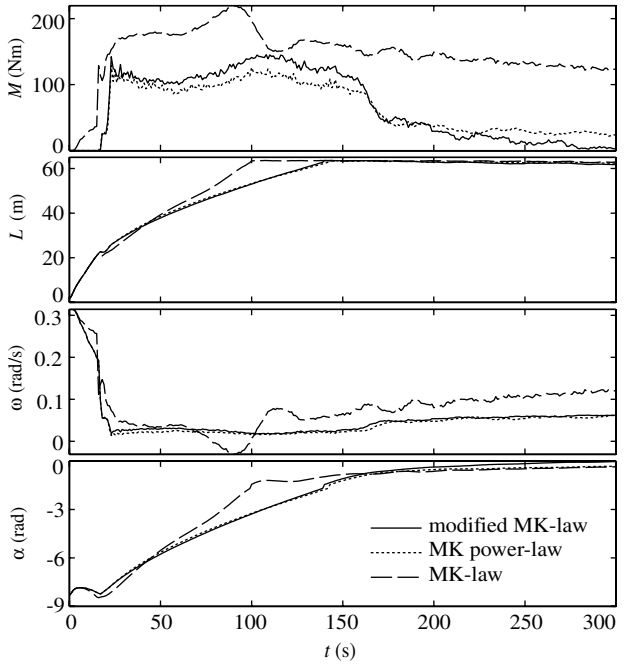

Fig. 9 FE simulations of space web deployment.

still increasing when the simulation ended. A higher ω_f implies increased centrifugal force, which requires increased material strength, and increased total angular momentum, which consumes more energy. Another important result is that ω decreased below zero, thus the hub changed direction of rotation, for the ordinary MK law, but not for the modified laws. The reason is that the new laws react faster to a change of ω when ω is small, even though the output torque can be kept lower. Finally, the deployment is slightly faster for the MK law if only $L \to L_{\max}$ is considered, but slower if $\alpha \to 0$ is taken into account.

Results for Deployment of Membranes Coiled on Spools

For the deployment of the LOFT [8], both the torque applied to the center hub and the tensile force in the spools, which is closely related to the deployment rate, were used as control parameters. The data for the LOFT were [8] $m_t = 149$ kg, $m_c = 227$ kg, $m_w = 282$ kg, $m_h = 1995$ kg, $R = 750$ m, $r = 2$ m, $\omega_0 = 1$ rad/s, and $\omega_f = 0.00916$ rad/s.

First, the deployment approach described by Hedgepeth [8] was employed. A constant torque of approximately 219 Nm was applied during the first 9500 s, before it was turned off. Thus, the angular momentum increased by 2.08×10^6 Nms, which is equal to the angular momentum required for the LOFT to spin uniformly at 0.00916 rad/s at the end of the deployment. Hedgepeth also discovered that a ramp-type tail-off of the torque reduced oscillations; therefore, the torque was linearly decreased here during 50 s at the end. Hedgepeth kept the total braking force constant at approximately 510 Nm when the torque was applied, then reduced it to a smaller value that enabled the LOFT to be deployed to its full size. Our results in Fig. 10 are in good agreement with the original results presented by Hedgepeth, even though all parameters required to repeat the simulations are not explicitly given in [8]. In the results, Hedgepeth did not show separate results for $\dot{\theta}$ and $\dot{\alpha}$, only for $\beta = \theta + \alpha$, and found transients only at the initiation of the deployment and at torque termination. However, the oscillations of the center hub, which are present in Fig. 10, may be detrimental for the deployment, even though the web is not oscillating.

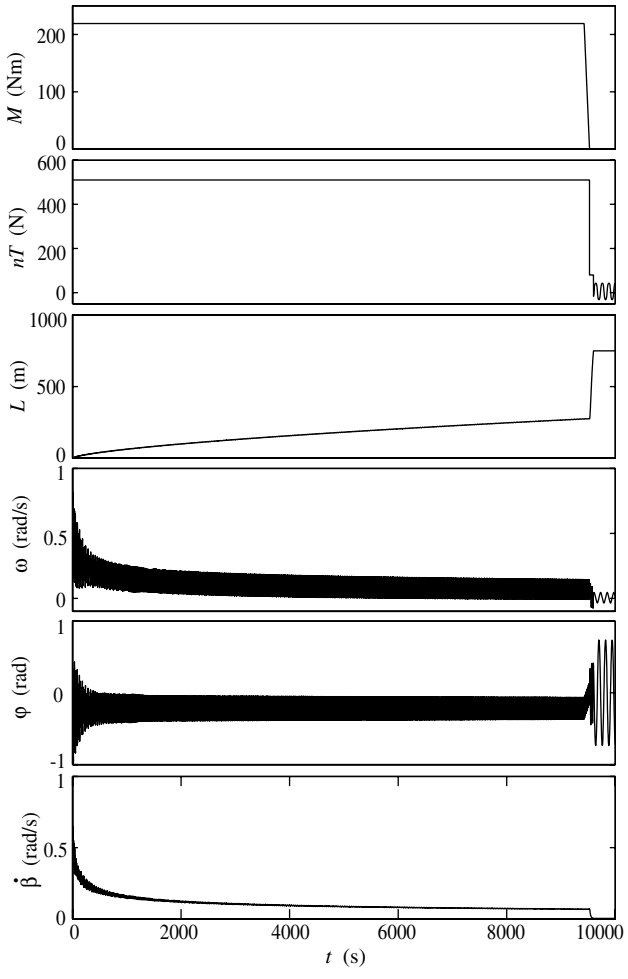

Fig. 10 LOFT deployment with Hedgepeth's control.

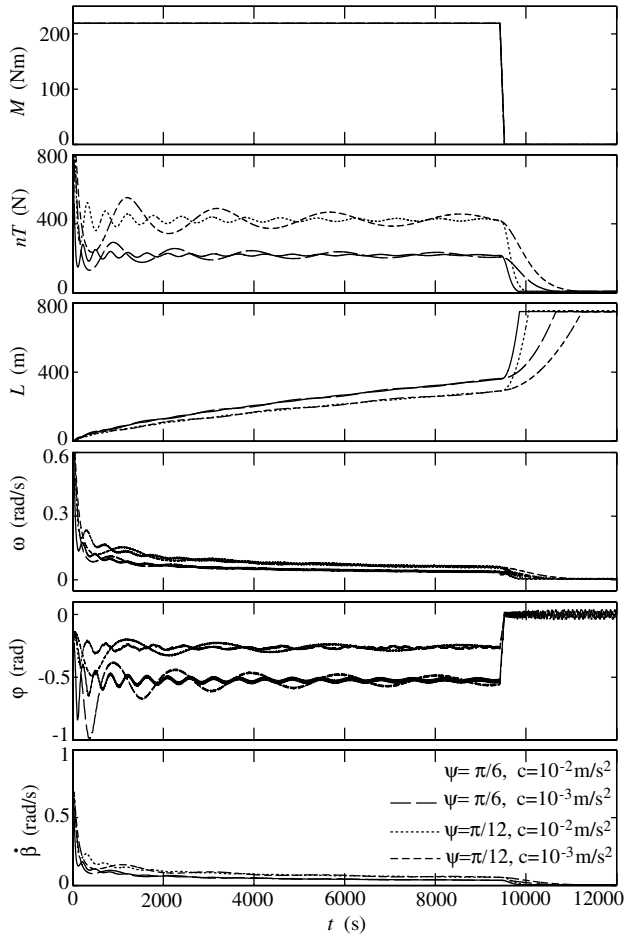

Fig. 11 LOFT deployment with feedback control.

Optimal Control of the Deployment

Unsuccessful attempts were made to optimize the LOFT deployment. It is more difficult to find converged optimal control laws, compared with when only torque was used, for several reasons:

1) There are more control and state variables.

2) It is more difficult to find a smooth initial guess because the control suggested in [8] yields an oscillating solution.

3) The Coriolis force limits the deployment rate because α is not allowed to exceed a certain value.

The main reason for the difficulty in finding a better solution may also be that Hedgepeth's control law already minimizes the integral of M, and for a given final time of 10,000 s, the integral of M^2 is also almost minimized, with complementing conditions on full deployment and final angular velocity.

Derivation of New Control Law from the Results

Compared with the original control by Hedgepeth, denoted as the H law, less transients and higher deployment rate during the first phase are desired. A constant torque is the most efficient way to increase the angular momentum for a given $M_{\max}$, and constant torque is probably advantageous for the electric motor. Therefore, it seems natural to instead focus on how to control the deployment velocity. A smaller braking force yields a faster deployment. At the same time, angular momentum must be transferred from the center hub to the membrane, and more angular momentum is transferred for a greater $|\varphi|$ or T. Also remember that for a membrane coiled on spools, $|\varphi| \geq \pi/6$ increases the risk for entanglement [9]. A compromise is to increase the deployment rate as long as $|\varphi|$ does not exceed a certain value ψ, which is acceptable for both deployment time and entanglement risk, and vice versa:

$$\ddot{L} = c(\psi - |\varphi|) \tag{40}$$

Simulation results obtained using (40), denoted as the modified H law, for the LOFT deployment are shown in Fig. 11. The high-frequency oscillations in ω and φ that were present in Fig. 10 are avoided. The derivatives $\dot{L}$ and $\dot{\varphi}$ oscillated with high frequency, but were allowed to do so. The deployment rate was higher in the first phase for a higher ψ. However, the main part of the deployment still occurred after the torque was terminated. The constant c, which determines how fast the deployment rate responds to a change in ψ, also determined the deployment rate in the second phase. A slower deployment may be desired in this phase to avoid springback, due to tether elasticity, at full deployment. The nontransient deployment of the second step was achieved due to the smooth decrease of T after the torque termination, which can probably also be obtained for other control laws (e.g., by letting T decrease as $L \rightarrow L_{\max}$). One drawback with the modified H law is that its success is strongly dependent on the parameters ψ and c, which must be obtained from simulations. The initial values $\dot{L}_0$ and ω_0 also have great influence on the results. Different parameters can be used for the two phases in which $M \neq 0$ and 0, respectively.

Conclusions

We have suggested dynamic models and optimal control laws for the centrifugal deployment of the webs and membranes in space. The dynamic models assume webs or membranes that are either 1) coiled around the hub and controlled by the angular velocity of the hub or 2) coiled on spools and controlled by the angular velocity of the hub and the deployment rate. The first coiling method has the advantages that it includes less mechanisms that can fail or cause entanglement, the deployment rate can be higher because the Coriolis force does not cause entanglement, and it is easier to coil a large web or membrane around the hub than onto smaller spools. The second method has the advantage that it includes more redundancy because such control can be used to limit the deployment rate, which could be important if ω decreases very rapidly toward zero. The second method is also advantageous for coiling reasons if split membranes are used.

For webs and membranes coiled on spools, a law similar to the H law can be used to obtain nontransient deployment. If the web or membrane is instead coiled around the center hub, one proposed control law introduces a power of the ω dependence of the MK law. Another proposed law suggests that ω_0 is replaced with ω_f in the MK law and $M = 0$ for $\omega \geq \omega_f$. The results show that the control laws based on the MK law are almost identical to the optimal control laws for certain parameter values, yet the simplicity of the MK law remains. The analytical model can be used to simulate the deployment and approximately determine the important $\hat{M}$ for the MK laws. Because of their simplicity, the MK laws can be implemented in FE software that allows feedback control or user-defined loads, which makes it possible to study the influence of perturbations or model imperfections. A safety margin on $\hat{M}$ may also be required for a real application, but a too-high $\hat{M}$ also gives rise to oscillations.

The response time from the measurement of the rotational velocity of the hub to the torque application was neglected. Should a significant time lag exist, it implies that the steep gradient of the torque, proposed by the optimal control and the modified MK laws for the early phase of the deployment, increases the risk of failure, especially because the torque gradient coincides with the most critical phase of the deployment (i.e., when $\omega \rightarrow 0$). To minimize this risk, a slow deployment should be chosen.

The new control strategies were derived for simple examples. However, the new control laws based on the MK law were useful also for the one-step deployment in the FE model, and so it is expected to be applicable to many different folding patterns and deployment schemes.

References

[1] Jones, T. C., Bart-Smith, H., Mikulas, M., and Watson, J., "Finite Element Modeling and Analysis of Large Pretensioned Space Structures," *Journal of Spacecraft and Rockets*, Vol. 44, No. 1, 2007, pp. 183–193.

doi:10.2514/1.23116
[2] Melnikov, V. M., and Pichkhadze, K. M., "Design of Frameless SA Deployed by Centrifugal Forces and Its Deployment Mechanism as a Basis of New Technology of In-Orbit Power Plant Assembling," *Proceedings of the 56th International Astronautical Congress*, Vol. 6, IAC-05-C2.P.01, International Astronautical Federation, Fukuoka, Japan, Oct. 2005, pp. 3972–3977.
[3] Schuerch, H. U., and MacNeal, R., "Deployable Centrifugally Stabilized Structures for Atmospheric Entry from Space," NASA CR-69, July 1964.
[4] Schuerch, H. U., and Hedgepeth, J. M., "Large Low-Frequency Orbiting Radio Telescope," NASA CR-1201, Oct. 1968.
[5] Robbins, W. M., Jr., "The Feasibility of an Orbiting 1500-Meter Radio Telescope," NASA CR-792, June 1967.
[6] MacNeal, R. H., "The Heliogyro: an interplanetary flying machine," NASA CR-84460, Mar. 1967.
[7] Lang, W. E., and Honeycutt, G. H., "Simulation of Deployment Dynamics of Spinning Spacecraft," NASA TN-D-4074, Aug. 1967.
[8] Hedgepeth, J. M., "Dynamics of a Large Spin-Stiffened Deployable Paraboloidal Antenna," *Journal of Spacecraft and Rockets*, Vol. 7, No. 9, 1970, pp. 1043–1048.
doi:10.2514/3.30100
[9] Melnikov, V. M., and Koshelev, V. A., *Large Space Structures Formed by Centrifugal Forces*, 1st ed., Earth Space Institute Book Series, Vol. 4, Gordon and Breach, Amsterdam, 1998, pp. 21–61.
[10] Shpakovsky, N., "Space Mirror," *The TRIZ Journal* [online journal], Vol. 7, No. 6, 2002, http://www.triz-journal.com/archives/2002/06/e/index.htm [retrieved 20 Feb. 2008].
[11] Wallace, R. A., Ayon, J. A., and Sprague, G. A., "Interstellar Probe Mission/System Concept," *IEEE Aerospace Conference Proceedings*, Vol. 7, Inst. of electrical and electronics Engineers, Piscataway, NJ, Mar. 2000, pp. 385–396.
[12] Salama, M., White, C., and Leland, R., "Ground Demonstration of a Spinning Solar Sail Deployment Concept," *Journal of Spacecraft and Rockets*, Vol. 40, No. 1, 2003, pp. 9–14.
doi:10.2514/2.3933
[13] Burton, R. L., Coverstone, V. L., Hargens-Rysanek, J., Ertmer, K. M., Botter, T., Benavides, G., Woo, B., Carroll, D. L., Gierow, P. A., Farmer, G., and Cardin, J., "Ultrasail—Ultra-Lightweight Solar Sail Concept," 41st AIAA/ASME/SAE/ASEE Joint Propulsion Conference, AIAA Paper 2005-4117, Tucson, AZ, July 2005.
[14] Mori, O., Tsuda, Y., Nishimura, Y., and Kawaguchi, J., "Deployment Dynamics of Clover Type Solar Sail," *Collection of Technical Papers. ISAS Workshop on Astrodynamics and Flight Mechanics*, Vol. 14, Inst. of Space and Astronautical Science, Japan Aerospace Exploration Agency, Kanagawa, Japan, 2005, pp. 25–31.
[15] Mitsugi, J., Natori, M., and Miura, K., "Preliminary Evaluation of the Spinning Solar Sail," 28th AIAA/ASME/ASCE/AHS/ASC Structures, Structural Dynamics, and Materials Conference, AIAA Paper 1987-742, Monterey, CA, Apr. 1987.
[16] Matunaga, S., Mori, O., Nakaya, K., Iai, M., Omagari, K., and Yabe, H., "New Spinning Deployment Method of Large Thin Membranes with Tether Control," *Proceedings of the 54th International Astronautical Congress*, Vol. 1, IAC-03-A.4.01, International Astronautical Federation, Bremen, Germany, Sept.–Oct. 2003, pp. 257–260.
[17] Matunaga, S., Yabe, H., Nakaya, K., Iai, M., Omagari, K., and Mori, O., "Membrane Deployment for Spinning Formation-Flight Solar Sail," *Collection of Technical Papers. ISAS Workshop on Astrodynamics and Flight Mechanics*, Vol. 14, Inst. of Space and Astronautical Science, Japan Aerospace Exploration Agency, Kanagawa, Japan, 2005, pp. 55–60.
[18] Arita, K., Hashiguchi, S., and Miyazaki, Y., "Evaluation of Deployment Method of Spin Deployable Membrane," *Proceedings of the 17th JAXA Workshop on Astrodynamics and Flight Mechanics*, Vol. 17, Inst. of Space and Astronautical Science, Japan Aerospace Exploration Agency, Kanagawa, Japan, 2007, pp. 251–254.
[19] Mori, O., Sawada, H., Tsuda, Y., Funase, R., Kawaguchi, J., Hanaoka, F., Matsumoto, M., Okada, S., Shibasaki, Y., Shirasawa, Y., Kitajima, A., Hirabayashi, M., Miwa, Y., Triwant, S., Arakawa, M., and Sugita, M., "Deployment Demonstration of Supersized Membrane for Spinning Solar Sail," *Proceedings of the 17th JAXA Workshop on Astrodynamics and Flight Mechanics*, Vol. 17, Inst. of Space and Astronautical Science, Japan Aerospace Exploration Agency, Kanagawa, Japan, 2007, pp. 245–250.
[20] Miyazaki, Y., "Dynamic Behavior of Spinning Solar Sail," 18th JAXA Workshop on Astrodynamics and Flight Mechanics, Japan Aerospace Exploration Agency, Paper A-7, 2008.
[21] Nakasuka, S., Funase, R., Nakada, K., Kaya, N., and Mankins, J. C., "Large Membrane 'Furoshiki Satellite' Applied to Phased Array Antenna and Its Sounding Rocket Experiment," *Acta Astronautica*, Vol. 58, No. 8, 2006, pp. 395–400.
doi:10.1016/j.actaastro.2005.12.010
[22] Nakasuka, S., Funane, T., Nakamura, Y., Nojira, Y., Sahara, H., Sasaki, F., and Kaya, N., "Sounding Rocket Flight Experiment for Demonstrating 'Furoshiki Satellite' for Large Phased Array Antenna," *Acta Astronautica*, Vol. 59, No. 1–5, 2006, pp. 200–205.
doi:10.1016/j.actaastro.2006.02.014
[23] Tibert, G., and Gärdsback, M., "Space Webs: Final Report," ESA, Advanced Concepts Team, Rept. 05/4109a, Noordwijk, The Netherlands, 2006.
[24] McKenzie, D., Cartmell, M., Radice, G., and Vasile, M., "Space Webs: Final Report," ESA, Advanced Concepts Team, Rept. 05/4109b, Noordwijk, The Netherlands, 2006.
[25] Palmerini, G. B., Sgubini, S., and Sabatini, M., "Space Webs Based on Rotating Tethered Formations," *Proceedings of the 57th International Astronautical Congress*, IAC-06-D1.1.04, International Astronautical Federation, Vol. 10, Oct. 2006, pp. 6819–6828.
[26] Gärdsback, M., Tibert, G., and Izzo, D., "Design Considerations and Deployment Simulations of Spinning Space Webs," *48th AIAA/ASME/ASCE/AHS/ASC Structures, Structural Dynamics, and Materials Conference*, Vol. 2, AIAA, Reston, VA, Apr. 2007, pp. 1503–1512; also AIAA Paper 2007-1829.
[27] McKenzie, D., and Cartmell, M., "Modelling of Tethered Space-Web Structures," *Journal of the British Interplanetary Society*, Vol. 61, Jan. 2008, pp. 24–31.
[28] Gärdsback, M., and Tibert, G., "Deployment Control of Spinning Space Webs," *Journal of Guidance, Control, and Dynamics*, Vol. 32, No. 1, 2009, pp. 40–50.
doi:10.2514/1.37468
[29] Miyazaki, Y., and Iwai, Y., "Dynamics Model of Solar Sail Membrane," *Collection of Technical Papers. ISAS Workshop on Astrodynamics and Flight Mechanics*, Vol. 14, Inst. of Space and Astronautical Science, Japan Aerospace Exploration Agency, Kanagawa, Japan, 2005, pp. 32–37.
[30] Kumar, K. D., "Review of Dynamics and Control of Nonelectrodynamic Tethered Satellite Systems," *Journal of Spacecraft and Rockets*, Vol. 43, No. 4, 2006, pp. 705–720.
doi:10.2514/1.5479
[31] Bainum, P. M., and Kumar, V. K., "Optimal Control of the Shuttle-Tethered- Subsatellite System," *Acta Astronautica*, Vol. 7, No. 12, 1980, pp. 1333–1348.
doi:10.1016/0094-5765(80)90010-7
[32] Fujii, H. A., and Anazawa, S., "Deployment/Retrieval Control of Tethered Subsatellite Through an Optimal Path," *Journal of Guidance, Control, and Dynamics*, Vol. 17, No. 6, 1994, pp. 1292–1298.
doi:10.2514/3.21347
[33] Barkow, B., Steidl, A., Troger, H., and Wiedermann, G., "Various Methods of Controlling the Deployment of a Tethered Satellite," *Journal of Vibration and Control*, Vol. 9, Nos. 1–2, 2003, pp. 187–208.
[34] Williams, P., "Optimal Deployment/Retrieval Of A Tethered Formation Spinning in the Orbital Plane," *Journal of Spacecraft and Rockets*, Vol. 43, No. 3, 2006, pp. 638–650.
doi:10.2514/1.17093
[35] Williams, P., "Optimal Deployment/Retrieval of Tethered Satellites," *Journal of Spacecraft and Rockets*, Vol. 45, No. 2, 2008, pp. 324–343.
doi:10.2514/1.31804
[36] Elnagar, J., Kazemi, M. A., and Razzaghi, M., "The Pseudospectral Legendre Method for Discretizing Optimal Control Problems," *IEEE Transactions on Automatic Control*, Vol. 40, No. 10, 1995, pp. 1793–1796.
doi:10.1109/9.467672
[37] Fahroo, F., and Ross, I. M., "Costate Estimation by a Legendre Pseudospectral Method," *Journal of Guidance, Control, and Dynamics*, Vol. 24, No. 2, 2001, pp. 270–277.
doi:10.2514/2.4709
[38] Kang, W., and Bedrossian, N., "Pseudospectral Optimal Control Theory Makes Debut Flight, Saves NASA $1M in Under Three Hours," *SIAM News* [online journal], Vol. 40, No. 7, 2007, http://www.siam.org/news/news.php?id=1196 [retrieved 30 Sept. 2007].
[39] Bergamin, L., and Izzo, D., "Comments on deployment and control of charged space webs," ACT, ACT-TNT-MAD-CDCCSW07, Noordwijk, The Netherlands, Sep. 2007.
[40] Blomquist, R., "Solar Blade Nanosatellite Development: Heliogyro Deployment, Dynamics and Control," 13th Annual AIAA/USU Conference on Small Satellites, Logan, UT, Utah State Univ. Paper VII-3, Aug. 1999.
[41] Conway, B., "Discrete Approximations to Optimal Trajectories Using Direct Transcription and Nonlinear Programming," *Journal of*

Guidance, Control, and Dynamics, Vol. 15, No. 4, 1992, pp. 994–1002. doi:10.2514/3.20934

[42] Trefethen, L., *Spectral Methods in MATLAB*, 1st ed., Society for Industrial and Applied Mathematics, Philadelphia, 2000.

[43] Gong, Q., Ross, I. M., Kang, W., and Fahroo, F., "Connections Between the Covector Mapping Theorem and Convergence of Pseudospectral Methods for Optimal Control," *Computational Optimization and Applications*, Vol. 41, No. 3, 2008, pp. 307–335. doi:10.1007/s10589-007-9102-4

[44] Ross, I. M., "User's Manual for DIDO: A MATLAB Application Package for Solving Optimal Control Problems," Naval Postgraduate School, TR MAE-03-005, Monterey, CA, Sept. 2003.

[45] Comsol Script, Software Package, Ver. 1.3.0.494, Comsol AB, Stockholm, 2008.

[46] Gill, P., Murray, W., and Saunders, M., "SNOPT: An SQP Algorithm for Large-Scale Constrained Optimization," *SIAM Journal on Optimization*, Vol. 12, No. 4, 2002, pp. 979–1006. doi:10.1137/S1052623499350013

[47] Comsol Optimization Lab, Software Package, Ver. 1.1, Comsol AB, Stockholm, 2007.

[48] Ross, I. M., and Fahroo, F., "Legendre Pseudospectral Approximations of Optimal Control Problems," *New Trends in Nonlinear Dynamics and Control and Their Applications*, Lecture Notes in Control and Information Sciences, Vol. 295, Springer, Berlin, 2004, pp. 327–342.

[49] Ross, I. M., *Space Trajectory Optimization and L1-Optimal Control Problems*, 1st ed., Butterworth-Heinemann, London, 2006, pp. 155–188.

[50] LS-DYNA, Software Package, Ver. 971/7600.1224, Livermore Software Technology Corp., Livermore, CA, 2007.

[51] Seely, L. G., Zimmerman, M., and McLaughlin, J., "The Use of Zylon Fibers in ULDB Tendons," *Advances in Space Research*, Vol. 33, No. 10, 2004, pp. 1736–1740. doi:10.1016/j.asr.2003.07.046

[52] MATLAB, Software Package, Ver. 7.5.0.338 (R2007b), The Mathworks, Inc., Natick, MA, 2007.